Chemosphere 299 (2022) 134334

Contents lists available at ScienceDirect

Chemosphere

journal homepage: www.elsevier.com/locate/chemosphere

Insights into Cr(VI) removal mechanism in water by facile one-step pyrolysis prepared coal gangue-biochar composite

Ruohan Zhao [a], Bing Wang [a,b,*], Xueyang Zhang [c], Xinqing Lee [d], Miao Chen [a], Qianwei Feng [a], Shiwan Chen [a]

[a] College of Resources and Environmental Engineering, Guizhou University, Guiyang, Guizhou, 550025, China
[b] Key Laboratory of Karst Georesources and Environment, Ministry of Education, Guiyang, Guizhou, 550025, China
[c] School of Environmental Engineering, Xuzhou University of Technology, Xuzhou, Jiangsu, 221000, China
[d] State Key Laboratory of Environmental Geochemistry, Institute of Geochemistry, Chinese Academy of Sciences, Guiyang, 550081, China

HIGHLIGHTS

- CG-RS was prepared by coal gangue co-pyrolysis with rape straw for Cr(VI) removal.
- CG-RS prepared at high pyrolysis temperature has maximum adsorption capacity (9.2 mg/g).
- CG-RS successfully loaded with Fe–O, Ca–O and Al–O functional groups.
- Reduction and surface complexation are the main mechanisms.

GRAPHICAL ABSTRACT

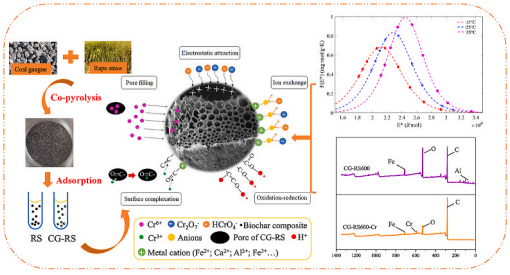

ARTICLE INFO

Handling Editor: X. Cao

Keywords:
Chromium
Solid waste
Site energy analysis
Wastewater treatment
Adsorption

ABSTRACT

The acceleration of industrialization has increased the discharge of chromium-containing wastewater, posing serious threat to the eco-environment and human health. To remove Cr(VI) in wastewater and improve resource utilization of solid waste, coal gangue and rape straw were initially used to prepare coal gangue-rape straw biochar (CG-RS) composite. The effects of pyrolysis temperatures, solution pH, coexisting ions of Cr(VI) adsorption were investigated. Different adsorption models combined with site energy analysis were used to explore the adsorption behaviors and mechanisms. The results showed higher pyrolysis temperature (600 °C) prepared CG-RS had a larger adsorption capacity (9.2 mg/g) for Cr(VI) (pH = 5.0). Analysis of XPS indicated that CG-RS successfully loaded with Fe–O and Al–O functional groups, which mainly participated in the reduction of Cr(VI). Site energy analysis further proved that reduction and surface complexation were the main adsorption mechanisms. This study shows an effective removal of Cr(VI) by CG-RS, providing a new way for resource utilization of solid waste.

* Corresponding author. College of Resources and Environmental Engineering, Guizhou University, Guiyang, Guizhou, 550025, China.
E-mail address: bwang6@gzu.edu.cn (B. Wang).

https://doi.org/10.1016/j.chemosphere.2022.134334
Received 17 January 2022; Received in revised form 7 March 2022; Accepted 13 March 2022
Available online 17 March 2022

1. Introduction

The acceleration of the industrialization process has resulted in the massive discharge of chromium (Cr)-containing wastewater (Xia et al., 2019). Cr is considered to be the first carcinogen in the environment, existing mainly as Cr(III) and Cr(VI) in water. Cr(III) is generally low-toxic, while Cr(VI) has extremely high toxicity (Liu et al., 2020b; Mishra et al., 2020). According to statistics of 2015, the discharge of Cr in the world has exceeded 105 tons (Shi et al., 2018), posing a serious threat to environment and human health. Therefore, the removal of Cr (VI) in wastewater is of great significance for water pollution.

As an effective method to remove heavy metals from water, adsorption has been used to remove Cr(VI) (Pakade et al., 2019; Fenti et al., 2020). Common adsorbents include synthetic polymers (Pakade et al., 2019), biochar (Wang et al., 2017), activated carbon (Wong et al., 2018), clay minerals (Gu et al., 2018), carbon nanotubes (Xu et al., 2018), nanoparticles and graphene (Sherlala et al., 2018), etc. Among them, biochar has been widely studied as a good adsorbent with the advantages of huge specific surface area (SSA), low cost, simple operation, and high adsorption capacity (Bolan et al., 2021). Biochar refers to a porous, highly aromatic and stable carbonaceous material produced by the pyrolysis of biomass materials under anaerobic or anaerobic conditions at a certain temperature (usually 300–700 °C) (Lehmann and Joseph, 2015). A large number of studies have applied it to remove pollutants in water, such as organic pollutants (Li et al., 2020), heavy metals (Cao et al., 2019), emerging pollutants (Cheng et al., 2021b), phosphate, and ammonium (Feng et al., 2022), etc. However, because most biochar is usually negatively charged, the adsorption capacity for anions is relatively limited. Therefore, how to improve the adsorption performance of biochar for oxygen anions is an urgent problem to be solved.

Previous studies have shown that with electrostatic attraction, surface reduction, complexation, and ion exchange, Cr(VI) can be adsorbed on the surface of biochar or converted into low-toxic Cr(III) (Gong et al., 2017; Liu et al., 2020b). For instance, Ma et al. (2021) used nZVI-pinecone biochar coupling with *Shewanella oneidensis MR-1* to improve the reduction and complexation of Cr(VI). They found that *MR-1* enhanced the adsorption capacity of Cr(VI), and Fe(II) played an important role in Cr(VI) reduction. Wan et al. (2019) found that Ca-alginate-nZVI-wheat bran biochar composite enhanced the adsorption capacity of Cr(VI) and reduced Fe leaching. Our previous studies have also found that due to the advantages of being rich in metal elements (such as Al and Fe) and high SSA, industrial solid waste modified biochar could effectively enhance the capacity of heavy metals, organic pollutants, and phosphate from water (Lian et al., 2019; Wang et al., 2020b; Zhao et al., 2021c). Cho et al. (2019) found that one-step pyrolysis prepared industrial solid waste (red mud)-lignin wastes biochar composite could apply to the removal of As(V), Cr(VI), and methylene blue, etc.. Therefore, we assumed that metal-containing industrial solid waste may improve the adsorption capacity and reduction of biochar on Cr(VI).

Coal gangue, as a common industrial solid waste, is generated during coal mining and washing. With a lot of Si, Al, and Fe content, the co-pyrolysis of coal gangue and biomass could potentially increase the forming of Fe–O, Al–O or other OFGs on biochar, as well as the electrical conductivity, pH, organic carbon content increased (Zhao et al., 2021c). At present, the studies of coal gangue modified biochar mainly focus on the adsorption of phosphate in water (Qiu and Duan, 2019; Wang et al., 2020b). Whether it can improve the adsorption capacity and reduction of Cr(VI) are not clear. In addition, although there have been some related studies on Cr(VI) by different biochar composites (Qian et al., 2017; Yin et al., 2020), the removal performance and mechanisms of Cr (VI) onto coal gangue-biochar are still not clarified. Using modern analysis technology combined with different adsorption models can help to reveal the mechanisms (Zhou et al., 2019; Cheng et al., 2021b; Zhao et al., 2021b).

To further explore the adsorption performance, influencing factors, and adsorption mechanisms of Cr(VI) onto coal gangue-biochar composite, the objectives of this study are to 1) prepare and characterize coal gangue-biochar composite; 2) analyze the factors affecting the adsorption process of Cr(VI); 3) explore the adsorption mechanisms by the combination of different adsorption models and site energy analysis.

2. Materials and methods

2.1. Reagents and materials

The coal gangue was mined from the mining area in Liupanshui City, Guizhou Province. Both rape and corn straws were taken from the suburbs of Guiyang City, Guizhou Province. Reagents used in the experiment are listed as follows: Diphenylcarbazide (AR, Chengdu Jinshan Chemical Reagent Co., Ltd., Sichuan, China); H_2SO_4, HCl, H_3PO_4, Na_2CO_3, Na_2SO_4, $NaNO_3$, NaCl (GR, Sinopharm Chemical Reagent Co., Ltd., Shanghai, China); Acetone (GR, Chongqing Chuandong Chemical Co., Ltd., Chongqing, China). Deionized water was used throughout the experiment.

2.2. Preparation of pristine biochar and coal gangue-biochar composite

The preparation method of rape straw biochar (RS) and coal gangue-rape straw biochar (CG-RS) composite was following the previous method (Lian et al., 2019). Rape straw was pyrolyzed at 300, 450, 600, 700 °C to obtain RS, labeled as RS300, RS450, RS600, and RS700. CG-RS was obtained as the same procedures with a mass ratio of 2:1, and labeled as CG-RS300, CG-RS450, CG-RS600, CG-RS700, respectively.

2.3. Characterization of samples

The conductivity of RS and CG-RS was measured by a conductivity meter (HI 8733, HANNA). X-ray diffraction (XRD) (Empyrean (Panaker Co., Ltd., Netherlands)) was used to determine the crystal structure of the two materials, $2\theta = 0°–60°$. The functional groups of RS and CG-RS were determined by Fourier transform infrared spectroscopy (FTIR) (Thermofisher, Nicolet iS10, USA). The surface elemental compositions of RS and CG-RS before and after Cr(VI) adsorption were identified by X-ray photoelectron spectroscopy (XPS) (Thermo Scientific K-Alpha+, ThermoFisher, China). The Malvern Zetasizer Nano ZSE (Malvern Instruments, UK) was measured Zeta potential. The SSA, porosity, and pore volume were determined by the Brunauer-Emmett-Teller method using Kubo X1000 analyzer (Beijing Builder Co., Ltd., China).

2.4. Adsorption experiments

A 50 mL PE centrifuge tube was used to perform all adsorption experiments at 22 ± 0.5 °C. The Cr(VI) standard solution was obtained by dissolving $K_2Cr_2O_7$ in deionized water. The concentration of Cr(VI) was analyzed according to our previous method (Lian et al., 2019). All samples were shaken in triplicate at 250 rpm for 24 h, and Cr(VI) was measured at 540 nm with Ultraviolet–visible Spectrophotometer (T6 New Century, Beijing Purse General Instrument Co., Ltd., Beijing, China).

To obtain the optimum pyrolysis temperatures and feedstocks, corn stalks biochar (CS), coal gangue-corn stalks biochar (CG-CS), RS, and CG-RS were prepared at pyrolysis temperatures of 300, 450, 600, 700 °C, respectively. To select the optimal adsorbent dosages, 0.025, 0.050, 0.100, 0.200, 0.500, and 1.000 g of RS and CG-RS were carried out in the adsorption experiments, respectively. To figure out the effect of solution pH on the adsorption process, 0.1 M NaOH and 0.1 M HCl solution were used to adjust the pH of 100 mg/L Cr(VI) solution to 3.0, 4.0, 5.0, 6.0, 7.0, 8.0, 9.0, 10.0. The adsorption kinetics of Cr(VI) were carried out in the time interval between 0.083 and 24 h. The adsorption isotherms of Cr(VI) were performed at an initial concentration of 5, 10,

25, 50, 100, 200, 300, 400, 500 mg/L and the adsorption thermodynamics were carried out at 15, 25, and 35 °C, respectively. The site energy analysis model was further adopted to analyze the main adsorption mechanisms (Zhou et al., 2019; Cheng et al., 2021a). The calculation formulas for site energy analysis are as follows (Yan et al., 2017):

$$E^* = -RT\ln(C_e / C_S) \quad (1)$$

$$F(E^*) = \frac{q_m nbC_s^n e^{\frac{-nE^*}{RT}}}{RT\left(1 + bC_s^n e^{\frac{-nE^*}{RT}}\right)^2} \quad (2)$$

T is the temperature in Kelvin, (K); R = 8.314 J/(mol·K); C_s is the maximum solubility of adsorbate in water (mg/L); E^* is the difference of adsorption energy at C_e and C_s, (kJ/mol).

3. Results and discussion

3.1. Characterization of samples

The basic physicochemical properties of RS600 and CG-RS600 are shown in Table 1. SSA of RS600 is 8.02 m^2/g, and CG-RS600 is 124.56 m^2/g. Coal gangue makes the surface of biochar have more pores and SSA, bringing more adsorption sites for Cr(VI) (Lian et al., 2019). Due to the alkalinity of coal gangue and biochar, the pH of CG-RS600 is slightly higher than pristine biochar. The Zero potential shows that the modification of coal gangue greatly increases the charges on the biochar surface, resulting in a significant increase in the changes of CG-RS600 at Zero potential. The Zeta potential values of the pristine biochar are all negative, while those of CG-RS600 are positive when the pH < 6.0. Therefore, under acidic conditions, positively charged CG-RS600 is beneficial to adsorb Cr(VI) in the form of anions in water.

The XRD patterns of RS600 and CG-RS600 before and after Cr(VI) adsorption are shown in Fig. 1a. Compared with the ray spectrum of RS600, the diffraction peaks of CG-RS600 have a significant increase. The modification of coal gangue increases the surface of RS600 with Al, Fe, and other elements, which can be observed in XPS spectra in Fig. 2. The increase of metal ions on the surface of CG-RS600 composite can enhance the ion exchange capacity, thereby promoting adsorption (Zhao et al., 2017; Qiu and Duan, 2019). In addition, the increased SiO_2 adds more OFGs to the surface of CG-RS600, which increases C═O, C═C, and other bond-to-bond reactions (Wang et al., 2020b).

Fig. 1b shows the infrared spectra of RS300, RS600, RS700, CG-RS300, CG-RS600, and CG-RS700. In Fig. 1b, the tensile variation of the peak around 3405 cm^{-1} indicates that –OH groups are on the surfaces of RS600 and CG-RS600. As the pyrolysis temperature increases, the active oxygen functional groups gradually weaken, indicating that the dehydrogenation reaction is intensified. The peaks from 2917 to 2859 cm^{-1} show the asymmetric and symmetric tensile vibrations of the methylene carbon on the surfaces of RS600 and CG-RS600 (Qiu et al., 2019). The peak fluctuations at 1588-1059 cm^{-1} are caused by the tensile vibration between bonds (such as –C═C, –C═O and –CH_3), which are significantly weaker or invisible at 600–700 °C than 300 °C, indicating that as the pyrolysis temperature increases, aliphatic hydrocarbons and OFGs are decomposed (Qian et al., 2017). It is more obviously that at 600 and 700 °C, CG-RS600 has a peak at 459 cm^{-1}, while pristine biochar does not have, indicating that the co-pyrolysis of coal gangue and biomass makes the surface of biochar successfully carry Si–O–Fe functional groups (Qiu et al., 2019; Wang et al., 2020b), which improves the adsorption capacity of Cr(VI). Meanwhile, the orbital peaks of Cr can be observed in the total XPS spectra of CG-RS600 before and after Cr(VI) adsorption in Fig. 2f, which proves that Cr(VI) has been successfully reduced and adsorbed onto the surface of CG-RS600 composite.

Table 1
Physiochemical properties of RS600 and CG-RS600.

Adsorbents	pH	Zeta potential (mV)	EC (μS/cm)	SSA (m^2/g)	Pore volume (cm^3/g)	Pore size (nm)
RS600	9.72	−17.55	917	8.02	0.004723	2.50
CG-RS600	9.85	−3.77	667	124.56	0.059436	2.28

3.2. Influencing factors

3.2.1. Effect of pyrolysis temperature

The pyrolysis temperature can affect the SSA and functional groups of biochar, thereby affecting adsorption performance (Wang et al., 2020a, 2020b). As the pyrolysis temperature increases, the number of micropores on the surface of biochar improves, and the SSA increases (Leng and Huang, 2018; Hassan et al., 2020). The SSA of CG-RS600 is 15.5 times that of RS600 (Table 1). The increased SSA provides more adsorption sites for the adsorption of Cr(VI) and increases the adsorption capacity. With the increase of pyrolysis temperature, the adsorption amount of Cr(VI) by RS and CG-RS shows an overall upward trend (Fig. 3a). Through the analysis of FTIR spectra of RS (Fig. 1b), peaks at 2917-2859 cm^{-1} and 1588-1059 cm^{-1} are corresponding to –CH_2, –C═C, –C═O, and –CH_3 (Qiu et al., 2019), respectively, which at 600–700 °C are significantly weaker or invisible than at 300 °C, proving that biochar prepared at low pyrolysis temperature contains more OFGs. Therefore, the pyrolysis temperature comprehensively affects the adsorption capacity of Cr(VI) by changing the SSA and functional groups of CG-RS composite. In this study, there is no significant difference in adsorption capacity on Cr(VI) of biochar pyrolyzed at 600 °C and 700 °C. In addition, adsorption capacities of RS and CG-RS with any pyrolysis temperatures are much higher than that of CS and CG-CS, respectively (Fig. 3a). Therefore, rape straw is selected as the optimum feedstock for the subsequent test.

3.2.2. Effect of adsorbent dosage

Fig. 3b shows the adsorption capacity and removal rate of RS600 and CG-RS600 on Cr(VI) under different dosages. With the dosage increases, the adsorption capacity of RS600 and CG-RS600 gradually decreases, while the removal rate is continuously increasing. Due to the continuous increase of the dosage, the SSA and adsorption sites of biochar continue to increase, and the corresponding functional groups also continue to increase. The overall removal rate shows an obvious upward trend with 0.05–0.20 g. While at 0.20–0.50 g, due to the limited initial concentration of pollutants, the upward trend begins to slow down. The removal rate of RS600 to Cr(VI) gradually stabilizes at 80%, while CG-RS600 exceeds 90%. Therefore, comprehensive consideration from an economic cost and adsorption efficiency perspective, 0.20 g is selected as the optimum dosage.

3.2.3. Effect of solution pH

Solution pH is considered to be the most important factor in the adsorption process of biochar (Wang et al., 2018). Fig. 3c shows the different adsorption capacities of RS600 and CG-RS600 for Cr(VI) under different pH. For RS600, when the pH increases from 3.0 to 4.0, the adsorption capacity has a significant increase. The adsorption capacity of CG-RS600 on Cr(VI) increases from pH 3.0 to 5.0, and then gradually decreases. In general, the adsorption capacity under acidic conditions is higher than that under alkaline conditions (Rajapaksha et al., 2018; Yin et al., 2020). The surface of RS600 is negatively charged, while pH < 6.0, the surface of CG-RS600 is positively charged (Fig. 3d). Cr(VI) mostly exists in the form of oxygen anions ($HCrO_4^-$, $Cr_2O_7^{2-}$) when pH < 6.0, which can be adsorbed in large quantities by CG-RS600 with positively charged. Therefore, the acidic condition is more suitable for the adsorption of Cr(VI) by CG-RS600. In addition, the original pH of Cr (VI) solution is about 5.0, considering the actual environment condition and cost, pH = 5.0 is the optimum condition for the removal of Cr(VI) in

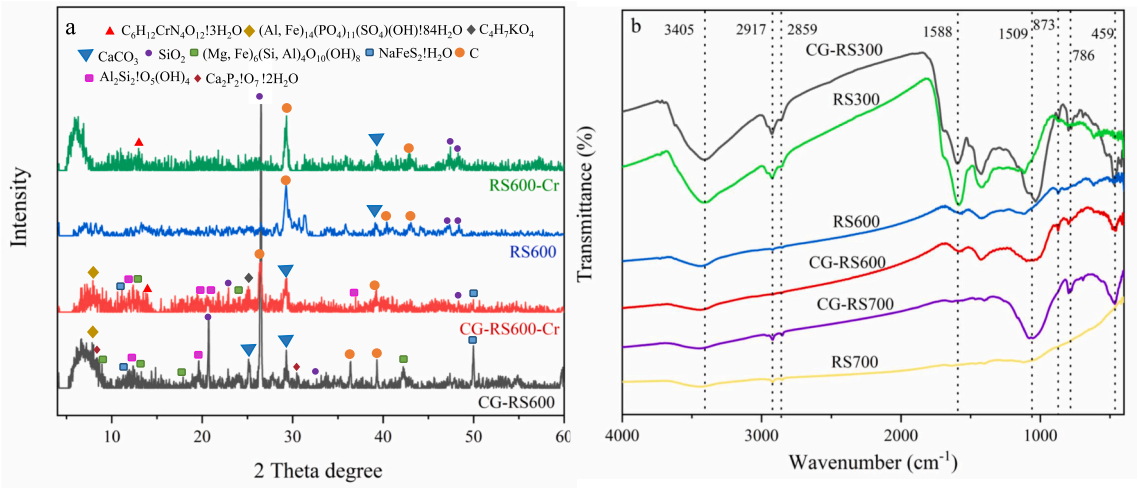

Fig. 1. XRD patterns (a) and the FTIR spectra of (b) of RS600 and CG-RS600.

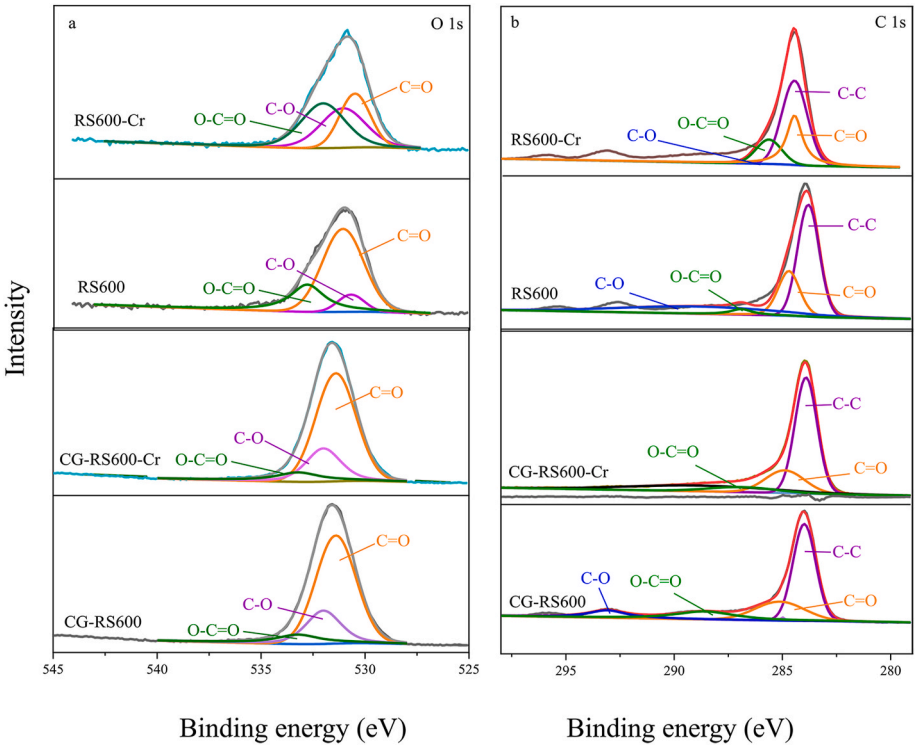

Fig. 2. XPS spectra of RS600 and CG-RS600 before and after Cr(VI) adsorption (a. O1s before and after adsorption; b. C1s before and after adsorption; c. Fe 2p of CG-RS600; d. Cr 2p of RS600; e. Cr 2p of CG-RS600; f. Total XPS spectra of CG-RS600 before and after adsorption; g. Total XPS spectra of RS600 before and after adsorption).

water.

3.2.4. *Coexisting ions*

In actual polluted wastewater, there are a large number of ions (CO_3^{2-}, SO_4^{2-}, NO_3^-, Cl^-) existing, which may form competitive adsorption with Cr(VI), affecting the adsorption capacity of CG-RS600 on Cr(VI). To explore the effects of anions on the adsorption capacity of CG-RS600 on Cr(VI) in actual wastewater, the adsorption capacity of Cr(VI) by CG-RS600 was evaluated in the presence of 0.001, 0.01, and 0.1 mol/L CO_3^{2-}, SO_4^{2-}, NO_3^- and Cl^- (Fig. 3e). It can be observed that high concentration (0.1 mol/L) of CO_3^{2-}, SO_4^{2-}, NO_3^- and Cl^- has positive effects on the Cr(VI) removal rate, while under low concentration, the removal rate of CG-RS600 for Cr(VI) remains almost unchanged in the coexistence of CO_3^{2-}, SO_4^{2-} and Cl^-. It is probably because CO_3^{2-}, SO_4^{2-} and NO_3^- could dissolve metal oxides (such as iron oxide or aluminum oxide) at high concentrations (Xu et al., 2021a), thus increasing the surface adsorption sites of CG-RS600. In addition, the dissolved metal oxide promotes the reduction of Cr(VI), promoting adsorption capacity.

3.3. *Adsorption kinetics*

Pseudo-second-order kinetics fitting curves of RS600 and CG-RS600 on Cr(VI) adsorption are shown in Fig. S1c. The adsorption rate of Cr(VI)

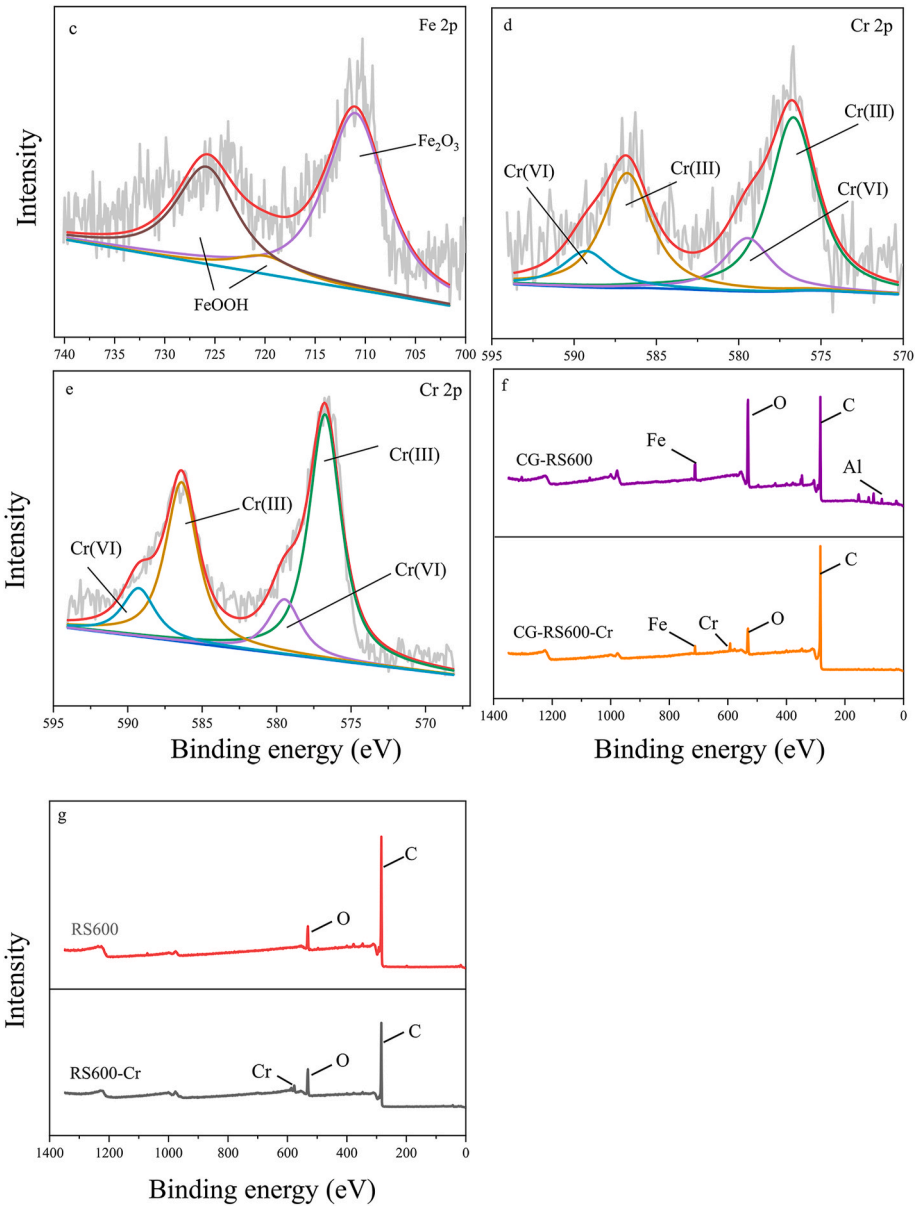

Fig. 2. (*continued*).

on RS600 and CG-RS600 is very fast in the first 4 h, which is because there are many adsorption sites on the surface of RS600 and CG-RS600 in the initial stage. As the time increases, the adsorption rate decreases significantly between 4 and 8 h, indicating that most of the adsorption sites have been occupied. Within 8–16 h, the adsorption capacity changes steadily, and the adsorption equilibrium is reached within 24 h.

Different kinetic models were used to fit the kinetic curves. From Table S1, the fitting correlation coefficient R^2 of the pseudo-second-order kinetic model is the highest, indicating that the pseudo-second-order kinetic model can better describe the Cr(VI) adsorption process. The equilibrium adsorption capacity calculated by the pseudo-second-order kinetic model is consistent with the actual equilibrium adsorption capacity. Therefore, The adsorption of CG-RS600 to Cr(VI) is mainly chemical adsorption, which is consistent with previous studies (Lian et al., 2019).

3.4. Adsorption isotherm

Two isotherm models of Freundlich and Langmuir were used to simulate the adsorption of Cr(VI) by RS600 and CG-RS600. Fig. S1a-b shows the adsorption isotherms of Cr(VI) on CG-RS600 and RS600. The amount of adsorption improves with the increase of the initial concentration. The adsorption capacity increases rapidly under low concentration, while the initial concentration of Cr(VI) increases, the adsorption capacity gradually reaches equilibrium. As the concentration of Cr(VI) increases, the surface-active sites of CG-RS600 are gradually occupied and reach a saturated state (Wang et al., 2020b). After the ambient temperature increases, the maximum adsorption capacity of Cr (VI) by CG-RS600 and RS600 also increases respectively, indicating that the ambient temperature can also affect the adsorption capacity of biochar (Wang et al., 2016a; Amen et al., 2020). Table S2 shows the fitting parameters of different adsorption isotherm models. The correlation coefficient of Langmuir fitting is higher than that of the Freundlich model, indicating that the Langmuir adsorption model can better fit the adsorption process of Cr(VI) on CG-RS600, proving the adsorption process is monolayer adsorption (Lian et al., 2019). The maximum adsorption capacity is 9.2 mg/g, which is twice the amount of pristine biochar. Compared with previous studies (Table 3), the maximum

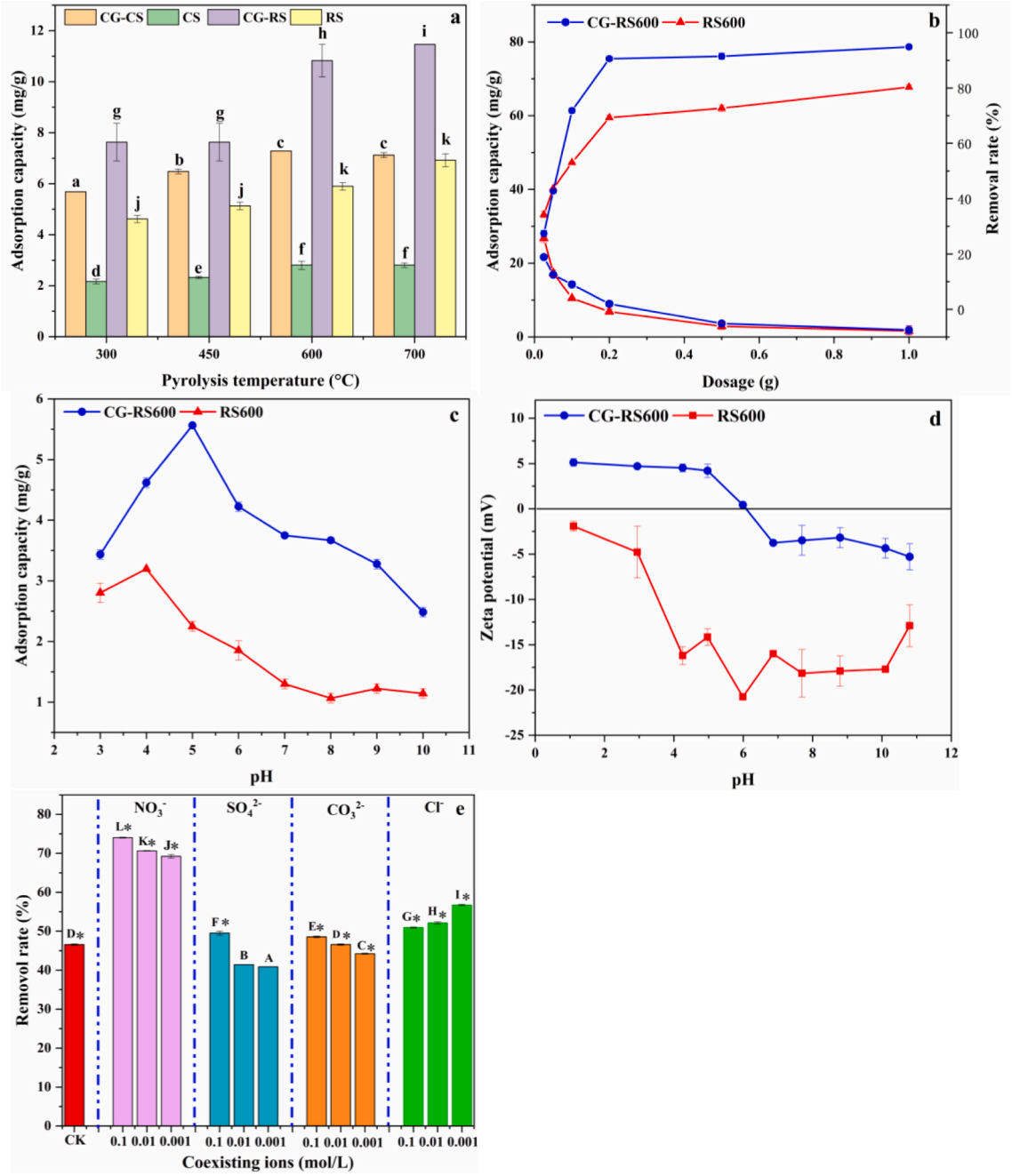

Fig. 3. Adsorption influencing factors of biochar and coal gangue-biochar composite on Cr(VI) with different pyrolysis temperatures (a), dosages (b), pH (c), Zeta potential (d), and coexisting ions (e) (Different letters denote significant differences for different pyrolysis temperature at $P < 0.05$. Symbols may cover the error bars. Each figure contains error bars, some too small to be visible.).

adsorption capacity of CG-RS600 on Cr(VI) is relatively high.

3.5. Adsorption thermodynamics

The thermodynamics of Cr(VI) adsorbed on CG-RS600 and RS600 at 289.15 K, 299.15 K and 309.15 K were analyzed. The thermodynamic parameters of RS600 are: $\triangle H = 0.410$ kJ/mol>0, $\triangle S = 103.268$ J/mol>0, $\triangle G = -29.741$ (15 °C), −30.774 (25 °C), −31.806 kJ/mol (35 °C) < 0; the thermodynamic parameters of CG-RS600 are: $\triangle H = 0.298$ kJ/mol>0, $\triangle S = 60.218$ J/mol, $\triangle G = -17.343$ (15 °C), −17.945 (25 °C), −18.547 kJ/mol (35 °C) < 0 (Table 2), indicating that the reactions are endothermic spontaneous. The higher ambient temperature makes the reaction occur more conducive. Under high

Table 2
Thermodynamic parameters of RS600 and CG-RS600 for Cr(VI) adsorption.

Adsorbents	T (K)	Langmuir isotherm		△G (kJ/mol)	△H (kJ/mol)	△S (kJ/mol·K)
		K_L (L/mg)	q_{max} (mg/g)			
RS600	288	0.169	2.1	−29.741	0.410	103.268
	298	0.100	3.2	−30.774		
	308	0.063	5.1	−31.806		
CG-RS600	288	0.043	6.3	−2.350	0.062	8.161
	298	0.040	8.0	−2.432		
	308	0.037	9.2	−2.514		

Table 3
The adsorption capacity of Cr(VI) in this study compared with previous studies.

Adsorbents	Pyrolysis temperature (°C)	Maximum adsorption capacity (mg/g)	pH	References
Pineapple peel biochar	700	7.44	4.0	Wang et al. (2016b)
Chitosan-magnetic Loofah biochar	700	30.14	3.0	Xiao et al. (2019)
Pine biochar	600–900	2.35	3.0	Zhao et al. (2021a)
Poplar biochar	675	5.40	5.0	He et al. (2019)
Soybean stover biochar	300	6.48	3.0	Rajapaksha et al. (2018)
Oak wood and oak bark biochar	400	4.93	2.0	Mohan et al. (2011)
CG-RS	600	9.20	5.0	This study

temperatures, the movement of molecules becomes more active, resulting in contact adsorption occurring more easily. $\triangle G < 0$ indicated that the reaction has higher spontaneity and stability (He et al., 2019). Therefore, the adsorption can be more promoted at high ambient temperatures. The absolute value of the standard enthalpy change is greater than 40 kJ/mol, indicating that the adsorption is dominated by chemical adsorption (Cheng et al., 2021a).

4. Adsorption mechanisms

The BET results of CG-RS600 and RS600 show that biochar at high pyrolysis temperature has a higher SSA and pore capacity, which is more conducive to the adsorption of Cr(VI), consistent with our previous research (Lian et al., 2019). According to the FTIR analysis of Fig. 1b, the modification of coal gangue causes the biochar to vibrate at 459 cm^{-1}, indicating that it has successfully carried Si–O–Fe on the surface of CG-RS600 (Wang et al., 2020b). In addition, the surface of RS600 and CG-RS600 contains abundant OFGs, which promotes the complexation of Cr(VI) on the surface of carbon materials, of which C═O and –COOH play major roles (Liu et al., 2020b; Zhong et al., 2021), thereby promoting adsorption.

According to Fig. 1a, metal salt crystals on the surface of CG-RS600 can be observed, which may promote the release of more cations into the solution. In this way, the surface adsorption sites of biochar are increased and the adsorption of Cr(III) is promoted (He et al., 2019). Therefore, the positive charge on the surface of CG-RS600 is increased, which improves the adsorption capacity of anions. And in the acidic range, Cr exists in the forms of $HCrO_4^-$ and $Cr_2O_7^{2-}$. The electron donor composed of polycyclic aromatic compounds and OFGs on the surface of CG-RS600 can effectively reduce Cr(VI) ((1)–(2)) (Lian et al., 2019). Therefore, under acidic conditions, the electrostatic attraction and ion exchange capacity between CG-RS600 and Cr(VI) are greatly increased, which promotes adsorption (Shi et al., 2018).

XPS spectra is also employed to analyze the adsorption mechanisms. The O1s spectra of the samples can be divided into 3 parts, which represent C═O, C–O, and O–C═O (Fig. 2b), while the 4 parts in C1s spectra represent C═C, C═O, C–O, and O–C═O (Fig. 2b) (Wu et al., 2021). Compared with RS600, the C═O content of CG-RS600 increases, indicating that carbonyl functional groups are introduced into biochar by coal gangue modification. For O1s and C1s spectras of CG-RS600, after reaction, the content of C–O reduces from 20.5% to 18.7%, O═C–O and C═O increase by 10% and 5% respectively, proving that OFGs participate in the redox process of Cr(VI) (Xu et al., 2019; Zhang et al., 2019). For spectras of RS600, the percentage of C═O decreases from 66% to 34%, that may be because the C═O group is oxidized by Cr (VI) (Tang et al., 2021). Fe 2p orbitals are observed in XPS spectra of CG-RS600, indicating that Fe in coal gangue is successfully loaded on the surface of biochar and form FeOOH and Fe_2O_3 with OFGs (Fig. 2c) (Liu et al., 2020c; Tang et al., 2021). These peaks almost disappear after adsorption, which proves that FeOOH participates in the reduction of Cr (VI) (Zhao et al., 2017; Liu et al., 2020a), and then forms stable crystal structures with Fe_2O_3 (Zou et al., 2021). In addition, the increased Fe (III), Fe(II), and Al(III) promote the electron transfer process on the surface of CG-RS600, which promotes the reduction process of Cr(VI) (Xu et al., 2021b; Yuan et al., 2022). The peaks of around 589 eV and 579 eV are characteristic of Cr $2p_{1/2}$ orbital of Cr(VI), while those around 586 eV and 576 eV are directed to Cr $2p_{1/2}$ orbital of Cr(III) (Fig. 2d and e) (Liu et al., 2020a), proving that Cr(VI) is successfully adsorbed to the surface of CG-RS600 (Xu et al., 2021a) and is reduced as Cr(III) (Rajapaksha et al., 2018). The orbital peaks of Cr, Fe, Al can also be observed in the total XPS spectra of CG-RS600 and RS600 before and after Cr(VI) adsorption in Fig. 2f and g.

In general, the mechanisms of biochar adsorption of Cr(VI) include the following processes (Fig. 4) (6–8): 1) under acidic conditions, due to the positive charges on the surface of CG-RS and a large amount of metal cations releasing, the Cr(VI) anions migrate to the positively charged biochar surface by electrostatic attraction; 2) the adsorbed Cr(VI) ions are reduced to Cr(III) by the electron donor composed of functional groups on the surface of CG-RS600; 3) the reduced Cr(III) reacts with C═O, Fe–O on the surface and forms stable Cr(III) with the surface of RS600 and CG-RS600.

$$HCrO_4^- + 7H^+ + 3e^- \rightarrow Cr^{3+} + 4H_2O \quad (6)$$

$$3C_xOH + Cr_2O_7^{2-} + 4H^+ \rightarrow 3C_xO + Cr^{3+} + 3H_2O \quad (7)$$

$$nCr^{3+} + (1-n)Fe^{3+} + 2H_2O \rightarrow Cr_nFe_{(1-n)}OOH + 3H^+ \quad (8)$$

To further figure out the adsorption mechanisms of CG-RS600 and RS600 on Cr(VI), site energy analysis was used. As shown in Fig. 5a and b, when the adsorption capacity of CG-RS600 composite on Cr(VI) increases, the E* value decreases, which indicates that $HCrO_4^-$ and $Cr_2O_7^{2-}$ firstly occupy the adsorption site with higher energy at low initial concentration (Sarkar et al., 2018). At higher ambient temperatures, more binding sites are activated, thereby increasing the adsorption capacity of CG-RS600 composite for Cr(VI) (Zhou et al., 2019).

The area under the curve of F (E*) and adsorption site energy reveals the number of available adsorption sites within a specific energy range (Reguyal and Sarmah, 2018). According to Fig. 5c and 5d, the frequency distribution of the energy of the adsorption site is an asymmetric single peak shape. At low adsorption site energy (<25 kJ/mol), the frequency distribution increases exponentially, and then decreases exponentially after reaching the highest frequency. Although the shape of the distribution function is similar, the area at different temperatures is significantly different. The adsorption sites of CG-RS600 composite on Cr(VI) are mainly concentrated between 20 and 26 kJ/mol, indicating that adsorption is mainly concentrated on high-energy sites. The interactions under high energy are mainly OFGs (carboxyl, hydroxyl, etc.) (Zhang et al., 2021). It is proved that the reduction and complexation of $HCrO_4^-$ and $Cr_2O_7^{2-}$ by oxygen-containing groups play major roles in the adsorption of CG-RS600 composite on Cr(VI), which further supports the above speculation about the adsorption mechanisms.

5. Conclusions

In this study, coal gangue-biochar composite was initially prepared by coal gangue and rape straw. The introduction of metal oxides from coal gangue improves the properties of CG-RS and promotes the adsorption of Cr(VI). High pyrolysis temperature increases the adsorption capacity of CG-RS (the maximum adsorption capacity: 9.2 mg/g). The adsorption process follows pseudo-second-order kinetics and Langmuir isotherm model. The site energy analysis model proves that

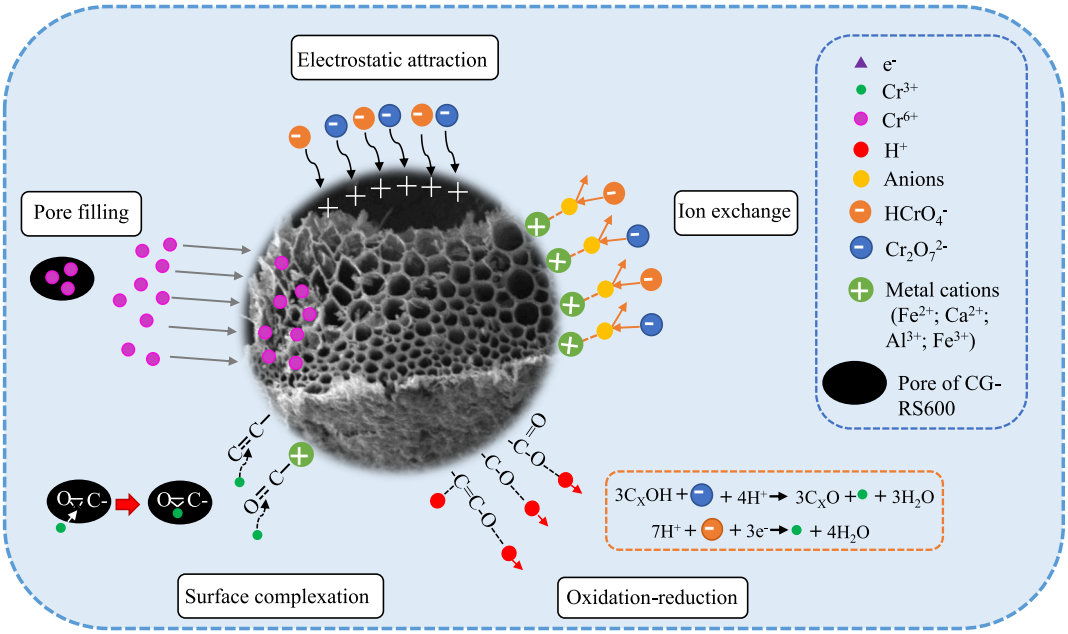

Fig. 4. The adsorption mechanisms of Cr(VI) onto CG-RS600.

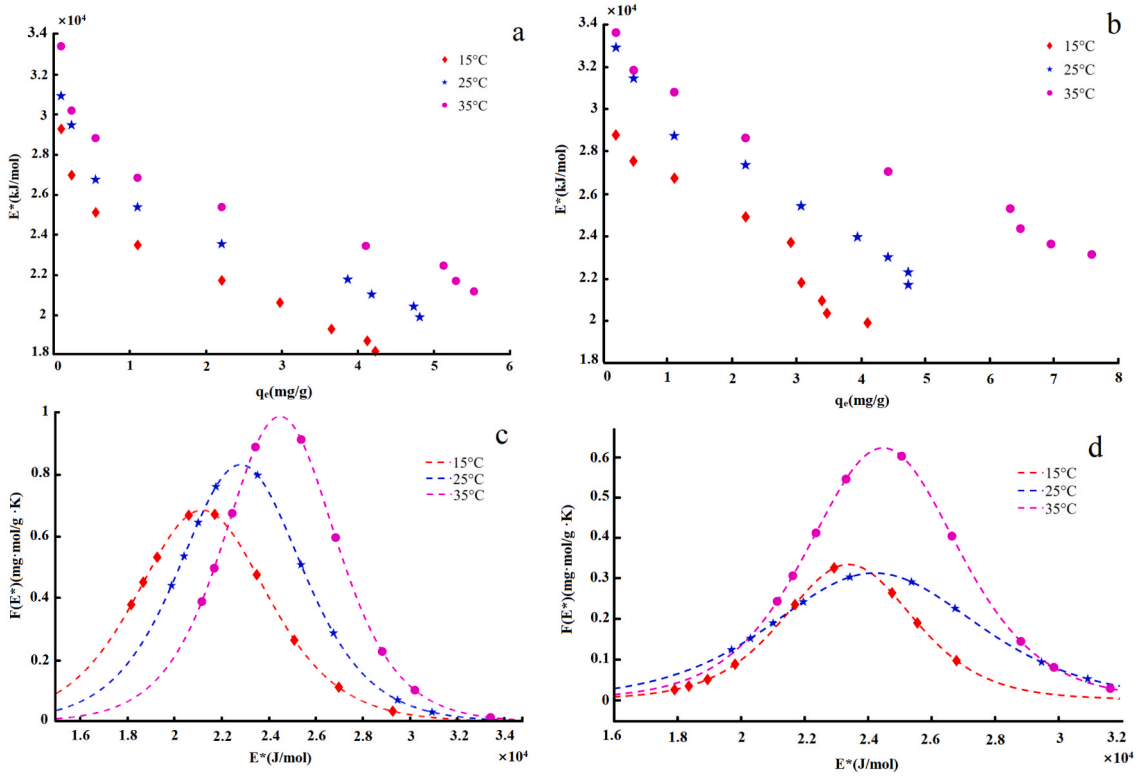

Fig. 5. The relationship between adsorption capacity and energy site of CG-RS600(a), RS600(b), and the site energy distribution of CG-RS600(c) and RS600(d).

reduction and surface complexation are the main adsorption mechanisms of Cr(VI) onto CG-RS600 composite. This study not only provides an effective method for Cr(VI) removal, but also realizes the resource utilization of solid waste.

Author contributions statement

Ruohan Zhao: Methodology, Formal analysis, Investigation, Writing-Review. Bing Wang: Conceptualization, Methodology, Formal analysis, Writing-Review &Editing. Xueyang Zhang: Experimental sample characterization. Xinqing Lee: Review &Editing. Miao Chen: Review &Editing. Qianwei Feng: Review &Editing. Shiwan Chen: Review &Editing.

Declaration of competing interest

The authors declare that they have no known competing financial interests or personal relationships that could have appeared to influence

the work reported in this paper.

Acknowledgments

This work was supported by the National Natural Science Foundation of China (41977297), the National Key Research and Development Program of China (2019YFC1805300), the Special Research Fund of Natural Science (Special Post) of Guizhou University [(2020)01], and the Key Cultivation Program of Guizhou University [2019(08)], the Project of Talent Base in Guizhou Province (RCJD2018-21).

Appendix A. Supplementary data

Supplementary data to this article can be found online at https://doi.org/10.1016/j.chemosphere.2022.134334.

References

Amen, R., Bashir, H., Bibi, I., Shaheen, S.M., Niazi, N.K., Shahid, M., Hussain, M.M., Antoniadis, V., Shakoor, M.B., Al-Solaimani, S.G., Wang, H., Bundschuh, J., Rinklebe, J., 2020. A critical review on arsenic removal from water using biochar-based sorbents: the significance of modification and redox reactions. Chem. Eng. J. 396 https://doi.org/10.1016/j.cej.2020.125195.

Bolan, N., Hoang, S.A., Beiyuan, J., Gupta, S., Hou, D., Karakoti, A., Joseph, S., Jung, S., Kim, K.H., Kirkham, M.B., Kua, H.W., Kumar, M., Kwon, E.E., Ok, Y.S., Perera, V., Rinklebe, J., Shaheen, S.M., Sarkar, B., Sarmah, A.K., Singh, B.P., Singh, G., Tsang, D.C.W., Vikrant, K., Vithanage, M., Vinu, A., Wang, H., Wijesekara, H., Yan, Y., Younis, S.A., Van Zwieten, L., 2021. Multifunctional applications of biochar beyond carbon storage. Int. Mater. Rev. 1–51.

Cao, Y., Xiao, W., Shen, G., Ji, G., Zhang, Y., Gao, C., Han, L., 2019. Carbonization and ball milling on the enhancement of Pb(II) adsorption by wheat straw: competitive effects of ion exchange and precipitation. Bioresour. Technol. 273, 70–76.

Cheng, N., Wang, B., Feng, Q., Zhang, X., Chen, M., 2021a. Co-adsorption performance and mechanism of nitrogen and phosphorus onto *eupatorium adenophorum* biochar in water. Bioresour. Technol. https://doi.org/10.1016/j.biortech.2021.125696.

Cheng, N., Wang, B., Wu, P., Lee, X., Xing, Y., Chen, M., Gao, B., 2021b. Adsorption of emerging contaminants from water and wastewater by modified biochar: a review. Environ. Pollut. 273 (15) https://doi.org/10.1016/j.envpol.2021.116448.

Cho, D.W., Yoon, K., Ahn, Y., Sun, Y., Tsang, C.W.D., Hou, D., Ok, Y.S., Song, H., 2019. Fabrication and environmental applications of multifunctional mixed metal-biochar composites (MMBC) from red mud and lignin wastes. J. Hazard Mater. 374, 412–419.

Feng, Q., Chen, M., Wu, P., Zhang, X., Wang, S., Yu, Z., Wang, B., 2022. Simultaneous reclaiming phosphate and ammonium from aqueous solutions by calcium alginate-biochar composite: sorption performance and governing mechanisms. Chem. Eng. J. 429 https://doi.org/10.1016/j.cej.2021.132166.

Fenti, A., Chianese, S., Iovino, P., Musmarra, D., Salvestrini, S., 2020. Cr(VI) sorption from aqueous solution: a review. Appl. Sci. 10 https://doi.org/10.3390/app10186477.

Gong, Y., Gai, L., Tang, J., Fu, J., Wang, Q., Zeng, E.Y., 2017. Reduction of Cr(VI) in simulated groundwater by FeS-coated iron magnetic nanoparticles. Sci. Total Environ. 595, 743–751.

Gu, S., Kang, X., Wang, L., Lichtfouse, E., Wang, C., 2018. Clay mineral adsorbents for heavy metal removal from wastewater: a review. Environ. Chem. Lett. 17, 629–654.

Hassan, M., Liu, Y., Naidu, R., Parikh, J., Sanjai, Du, J., Qi, F., Willett, R.I., 2020. Influences of feedstock sources and pyrolysis temperature on the properties of biochar and functionality as adsorbents: a meta-analysis. Sci. Total Environ. 744 https://doi.org/10.1016/j.scitotenv.2020.140714.

He, R., Yuan, X., Huang, Z., Wang, H., Jiang, L., Huang, J., Tan, M., Li, H., 2019. Activated biochar with iron-loading and its application in removing Cr(VI) from aqueous solution. Colloids Surf. A Physicochem. Eng. Asp. 579 https://doi.org/10.1016/j.colsurfa.2019.123642.

Lehmann, J., Joseph, S., 2015. Biochar for Environmental Management: Science, Technology and Implementation. Routledge, New York.

Leng, L., Huang, H., 2018. An overview of the effect of pyrolysis process parameters on biochar stability. Bioresour. Technol. 270, 627–642.

Li, Y., Zimmerman, A.R., He, F., Chen, J., Han, L., Chen, H., Hu, X., Gao, B., 2020. Solvent-free synthesis of magnetic biochar and activated carbon through ball-mill extrusion with Fe_3O_4 nanoparticles for enhancing adsorption of methylene blue. Sci. Total Environ. 722 https://doi.org/10.1016/j.scitotenv.2020.137972.

Lian, G., Wang, B., Lee, X., Li, L., Liu, T., Lyu, W., 2019. Enhanced removal of hexavalent chromium by engineered biochar composite fabricated from phosphogypsum and distillers grains. Sci. Total Environ. 697 https://doi.org/10.1016/j.scitotenv.2019.134119.

Liu, L., Liu, X., Wang, D., Lin, H., Huang, L., 2020a. Removal and reduction of Cr(Vl) in simulated wastewater using magnetic biochar prepared by co-pyrolysis of nano-zero-valent iron and sewage sludge. J. Clean. Prod. 257 https://doi.org/10.1016/j.jclepro.2020.120562.

Liu, N., Zhang, Y., Xu, C., Liu, P., Lv, J., Liu, Y., Wang, Q., 2020b. Removal mechanisms of aqueous Cr(VI) using apple wood biochar: a spectroscopic study. J. Hazard Mater. 384 https://doi.org/10.1016/j.jhazmat.2019.121371.

Liu, X., Yang, L., Zhao, H., Wang, W., 2020c. Pyrolytic production of zerovalent iron nanoparticles supported on rice husk-derived biochar: simple, in situ synthesis and use for remediation of Cr(VI)-polluted soils. Sci. Total Environ. 708 https://doi.org/10.1016/j.scitotenv.2019.134479.

Ma, L., Du, Y., Chen, S., Du, D., Ye, H., Zhang, T.C., 2021. Highly efficient removal of Cr (VI) from aqueous solution by pinecone biochar supported nanoscale zero-valent iron coupling with *Shewanella oneidensis MR-1*. Chemosphere 287. https://doi.org/10.1016/j.chemosphere.2021.132184.

Mishra, A., Gupta, B., Kumar, N., Singh, R., Varma, A., Thakur, I.S., 2020. Synthesis of calcite-based bio-composite biochar for enhanced biosorption and detoxification of chromium Cr(VI) by *Zhihengliuella sp. ISTPL4*. Bioresour. Technol. 307 https://doi.org/10.1016/j.biortech.2020.123262.

Mohan, D., Rajput, S., Singh, V.K., Steele, P.H., Pittman Jr., C.U., 2011. Modeling and evaluation of chromium remediation from water using low cost bio-char, a green adsorbent. J. Hazard Mater. 188, 319–333.

Pakade, V.E., Tavengwa, N.T., Madikizela, L.M., 2019. Recent advances in hexavalent chromium removal from aqueous solutions by adsorptive methods. RSC Adv. 9, 26142–26164.

Qian, L., Zhang, W., Yan, J., Han, L., Chen, Y., Ouyang, D., Chen, M., 2017. Nanoscale zero-valent iron supported by biochars produced at different temperatures: synthesis mechanism and effect on Cr(VI) removal. Environ. Pollut. 223, 153–160.

Qiu, B., Duan, F., 2019. Synthesis of industrial solid wastes/biochar composites and their use for adsorption of phosphate: from surface properties to sorption mechanism. Colloids Surf., A 571, 86–93.

Qiu, B., Duan, F., He, G., 2019. Value adding industrial solid wastes: impact of industrial solid wastes upon copper removal performance of synthesized low cost adsorbents. Energy Sources, Part A Recovery, Util. Environ. Eff. 42, 835–848.

Rajapaksha, A.U., Alam, M.S., Chen, N., Alessi, D.S., Igalavithana, A.D., Tsang, D.C.W., Ok, Y.S., 2018. Removal of hexavalent chromium in aqueous solutions using biochar: chemical and spectroscopic investigations. Sci. Total Environ. 625, 1567–1573.

Reguyal, F., Sarmah, A.K., 2018. Site energy distribution analysis and influence of Fe_3O_4 nanoparticles on sulfamethoxazole sorption in aqueous solution by magnetic pine sawdust biochar. Environ. Pollut. 233, 510–519.

Sarkar, A., Ranjan, A., Paul, B., 2018. Synthesis, characterization and application of surface-modified biochar synthesized from rice husk, an agro-industrial waste for the removal of hexavalent chromium from drinking water at near-neutral pH. Clean Technol. Environ. Policy 21, 447–462.

Sherlala, A.I.A., Raman, A.A.A., Bello, M.M., Asghar, A., 2018. A review of the applications of organo-functionalized magnetic graphene oxide nanocomposites for heavy metal adsorption. Chemosphere 193, 1004–1017.

Shi, S., Yang, J., Liang, S., Li, M., Gan, Q., Xiao, K., Hu, J., 2018. Enhanced Cr(VI) removal from acidic solutions using biochar modified by Fe_3O_4@SiO_2-NH_2 particles. Sci. Total Environ. 628–629, 499–508.

Tang, J., Zhao, B., Lyu, H., Li, D., 2021. Development of a novel pyrite/biochar composite (BM-FeS_2@BC) by ball milling for aqueous Cr(VI) removal and its mechanisms. J. Hazard Mater. 413 https://doi.org/10.1016/j.jhazmat.2021.125415.

Wan, Z., Cho, D.W., Tsang, D.C.W., Li, M., Sun, T., Verpoort, F., 2019. Concurrent adsorption and micro-electrolysis of Cr(VI) by nanoscale zerovalent iron/biochar/Ca-alginate composite. Environ. Pollut. 247, 410–420.

Wang, B., Gao, B., Fang, J., 2017. Recent advances in engineered biochar productions and applications. Crit. Rev. Environ. Sci. Technol. 47, 2158–2207.

Wang, B., Lehmann, J., Hanley, K., Hestrin, R., Enders, A., 2016a. Ammonium retention by oxidized biochars produced at different pyrolysis temperatures and residence times. RSC Adv. 6, 41907–41913.

Wang, B., Lian, G., Lee, X., Gao, B., Li, L., Liu, T., Zhang, X., Zheng, Y., 2020a. Phosphogypsum as a novel modifier for distillers grains biochar removal of phosphate from water. Chemosphere 238. https://doi.org/10.1016/j.chemosphere.2019.124684.

Wang, B., Ma, Y., Lee, X., Wu, P., Liu, F., Zhang, X., Li, L., Chen, M., 2020b. Environmental-friendly coal gangue-biochar composites reclaiming phosphate from water as a slow-release fertilizer. Sci. Total Environ. https://doi.org/10.1016/j.scitotenv.2020.143664.

Wang, C., Gu, L., Liu, X., Zhang, X., Cao, L., Hu, X., 2016b. Sorption behavior of Cr(VI) on pineapple-peel-derived biochar and the influence of coexisting pyrene. Int. Biodeterior. Biodegrad. 111, 78–84.

Wang, Q., Wang, B., Lee, X., Lehmann, J., Gao, B., 2018. Sorption and desorption of Pb (II) to biochar as affected by oxidation and pH. Sci. Total Environ. 634, 188–194.

Wong, S., Ngadi, N., Inuwa, I.M., Hassan, O., 2018. Recent advances in applications of activated carbon from biowaste for wastewater treatment: a short review. J. Clean. Prod. 175, 361–375.

Wu, J., Wang, T., Wang, J., Zhang, Y., Pan, W.P., 2021. A novel modified method for the efficient removal of Pb and Cd from wastewater by biochar: enhanced the ion exchange and precipitation capacity. Sci. Total Environ. 754 https://doi.org/10.1016/j.scitotenv.2020.142150.

Xia, S., Song, Z., Paramsothy, J., Sabry, M.S., Jörg, R., Yong, S.O., Nanthi, B., Wang, H., 2019. A critical review on bioremediation technologies for Cr(VI)-contaminated soils and wastewater. Crit. Rev. Environ. Sci. Technol. 49, 1027–1078.

Xiao, F., Cheng, J., Cao, W., Yang, C., Chen, J., Luo, Z., 2019. Removal of heavy metals from aqueous solution using chitosan-combined magnetic biochars. J. Colloid Interface Sci. 540, 579–584.

Xu, H., Gao, M., Hu, X., Chen, Y., Li, Y., Xu, X., Zhang, R., Yang, X., Tang, C., Hu, X., 2021a. A novel preparation of S-nZVI and its high efficient removal of Cr(VI) in aqueous solution. J. Hazard Mater. 416 https://doi.org/10.1016/j.jhazmat.2021.125924.

Xu, J., Cao, Z., Zhang, Y., Yuan, Z., Lou, Z., Xu, X., Wang, X., 2018. A review of functionalized carbon nanotubes and graphene for heavy metal adsorption from water: preparation, application, and mechanism. Chemosphere 195, 351–364.

Xu, X., Huang, H., Zhang, Y., Xu, Z., Cao, X., 2019. Biochar as both electron donor and electron shuttle for the reduction transformation of Cr(VI) during its sorption. Environ. Pollut. 244, 423–430.

Xu, Z., Xu, X., Yu, Y., Yao, C., Tsang, D.C.W., Cao, X., 2021b. Evolution of redox activity of biochar during interaction with soil minerals: effect on the electron donating and mediating capacities for Cr(VI) reduction. J. Hazard Mater. 414 https://doi.org/10.1016/j.jhazmat.2021.125483.

Yan, B., Niu, C.H., Wang, J., 2017. Kinetics, electron-donor-acceptor interactions, and site energy distribution analyses of norfloxacin adsorption on pretreated barley straw. Chem. Eng. J. 330, 1211–1221.

Yin, Z., Xu, S., Liu, S., Xu, S., Li, J., Zhang, Y., 2020. A novel magnetic biochar prepared by K_2FeO_4-promoted oxidative pyrolysis of pomelo peel for adsorption of hexavalent chromium. Bioresour. Technol. 300 https://doi.org/10.1016/j.biortech.2019.122680.

Yuan, Y., Zhou, M., Shi, J., Zhang, C., Zhang, J., Rinklebe, J., Yin, W., Wang, S., Wang, X., 2022. The significant role of electron donating capacity and carbon structure of biochar to electron transfer of zerovalent iron. Chemosphere 287, 132381.

Zhang, S., Lyu, H., Tang, J., Song, B., Zhen, M., Liu, X., 2019. A novel biochar supported CMC stabilized nano zero-valent iron composite for hexavalent chromium removal from water. Chemosphere 217, 686–694.

Zhang, X., Chu, Y., Zhang, H., Hu, J., Wu, F., Wu, X., Shen, G., Yang, Y., Wang, B., Wang, X., 2021. A mechanistic study on removal efficiency of four antibiotics by animal and plant origin precursors-derived biochars. Sci. Total Environ. 772 https://doi.org/10.1016/j.scitotenv.2021.145468.

Zhao, J., Boada, R., Cibin, G., Palet, C., 2021a. Enhancement of selective adsorption of Cr species via modification of pine biomass. Sci. Total Environ. 756, 143816.

Zhao, L., Ding, Z., Sima, J., Xu, X., Cao, X., 2017. Development of phosphate rock integrated with iron amendment for simultaneous immobilization of Zn and Cr(VI) in an electroplating contaminated soil. Chemosphere 182, 15–21.

Zhao, N., Zhao, C., Liu, K., Zhang, W., Tsang, D.C.W., Yang, Z., Yang, X., Yan, B., Morel, J.L., Qiu, R., 2021b. Experimental and DFT investigation on N-functionalized biochars for enhanced removal of Cr(VI). Environ. Pollut. 291 https://doi.org/10.1016/j.envpol.2021.118244.

Zhao, R., Wang, B., Theng, B.K.G., Wu, P., Liu, F., Lee, X., Chen, M., Sun, J., 2021c. Fabrication and environmental applications of metal-containing solid waste/biochar composites: A review. Science of the Total Environment. https://doi.org/10.1016/j.scitotenv.2021.149295.

Zhong, M., Li, M., Tan, B., Gao, B., Qiu, Y., Wei, X., Hao, H., Xia, Z., Zhang, Q., 2021. Investigations of Cr(VI) removal by millet bran biochar modified with inorganic compounds: momentous role of additional lactate. Sci. Total Environ. 793, 148098.

Zhou, Y., He, Y., He, Y., Liu, X., Xu, B., Yu, J., Dai, C., Huang, A., Pang, Y., Luo, L., 2019. Analyses of tetracycline adsorption on alkali-acid modified magnetic biochar: site energy distribution consideration. Sci. Total Environ. 650, 2260–2266.

Zou, H., Zhao, J., He, F., Zhong, Z., Huang, J., Zheng, Y., Zhang, Y., Yang, Y., Yu, F., Bashir, M.A., Gao, B., 2021. Ball milling biochar iron oxide composites for the removal of chromium (Cr(VI)) from water: performance and mechanisms. J. Hazard Mater. 413, 125252.